J A S T
Journal of Aerospace Science and Technology

Simulation of Pitching and Heaving Airfoil with Oscillation of Flow Boundary Condition

M. H. Djavareshkian[1*] and A. M. Faghihi[2]

1, 2. Faculty of Engineering, Department of Mechanical Engineering, Ferdowsi University of Mashhad

*P.O. Box: 95775-1111, Mashhad, IRAN

Javareshkian@um.ac.ir

A pressure based implicit procedure to solve the Euler and Navier-Stokes equations is developed to predict transonic viscous and inviscid flows around the pitching and heaving airfoils with a high resolution scheme. In this process, nonorthogonal and non moving mesh with collocated finite volume formulation are used. In order to simulate pitching or heaving airfoil, oscillation of flow boundary condition is applied. The boundedness criteria for this procedure are determined from Normalized Variable Diagram (NVD) scheme. The procedure incorporates the k-ε eddy-viscosity turbulence model. This process is tested for inviscid and turbulent transonic aerodynamic flows around oscillation airfoil. The results are compared with other existing numerical solutions and with the experimental data. The comparisons show that the resolution quality of the developed algorithm is significant.

Keywords: Pitching, Heaving, Transonic, Inviscid, Viscous, Boundary condition

NOMENCLATURE

D	Finite difference coefficient
C_μ, C_1, C_2	Empirical coefficient
I	Flux
q	Scalar flux vector
T	Stress tensor
u, v	Mean (time average) velocity components in x and y directions, respectively
Γ	Diffusivity coefficients
δv	Cell volume
ε	Volumetric rate of dissipation
μ	Dynamic viscosity
μ_t	Turbulent viscosity
ρ	Density
σ_k	Turbulent Prandtl number for turbulent Kinetic energy
σ_ε	Turbulent Prandtl number for dissipation rate
ϕ	Scalar quantity
κ	Reduced frequency=$\omega c/(2V_\infty)$

V_∞	Free stream velocity
α	Angle of attack
f	Physical frequency
α	Angle of attack in mean position
ω_a	Circular frequency,$2\pi f$
AMP	Amplitude
SBIC	Second and Blending Interpolation Combine

INTRODUCTION

The unsteady aerodynamics of pitching and heaving airfoils has principally two traditional motivating applications: one is the engineering application of dynamic stall of aircraft lifting surfaces in aggressive maneuver, and of helicopter blades. The other one is the aerodynamics of flapping wings in swimming and flying animals. In both cases, abstractions to sinusoidal pitching and heaving of nominally two dimensional airfoils have been useful for studying the evolution of vortex shedding, the time dependency of aerodynamic loads. Generally, the simulation of oscillating airfoil is done in

1. Associate Professor (Corresponding Author)
2. phD Student

two ways. In the first method, the airfoil is oscillated while the flow is steady. In this case the dynamic mesh is used. In the second method, the oscillatory inlet flow is passing on a fixed airfoil.

In the field of simulating moving boundary flow problems, different approaches are found in the literature of the art. Shankar and Ide [1] have presented an appropriate grid update procedure for small displacements of the structure where the speeds of the outer boundary points are taken to be zero and the grid speeds at any interior point are then obtained by interpolating the body value and the zero outer boundary value along a constant coordinate line. However, this method may result in severe grid distortions when the structure experiences large displacements. Goswami and Parpia [2] mentioned that local grid restructuring methods can be used when at each time step, the boundary movement is smaller than the minimum mesh size in the domain. In order to rectify the high cost of mesh insertion and deletion in the previous method, Batina [3] introduced dynamic mesh approach. This method employs mesh smoothing instead of insertion and deletion of near boundary grids. The process of Mesh smoothing is implemented until a proper mesh quality, which is based on several criteria, is achieved [4]. In order to attain a pattern for grid points to satisfy a set of smoothness and orthogonality constraints, Nakahashi and Deiwert [5] used the concept of spring coupled with variation principles. Levine et al. [6] utilized a similar spring analogy to compute the new body conforming grid points. Guruswamy [7] introduced a dynamic algebraic grid generation scheme in which grid points are conformed to the deforming shapes of the structure. Lohner [8] proposed the use of Arbitrary Lagrangian-Eulerian (ALE) formulation as a means to achieve a solver that can handle moving frames. However, the grid points in ALE formulation had to be renewed even in the sheer rigid-body motion problems. Additionally, Farhat and Lin [9] introduced a more economical approach for transient solution of the aero elastic coupled problem with respect to multiple moving frames of reference.

Other approaches to handling moving boundary problems are also available. The field velocity method (Parameswaran and Baeder, [10], Singh and Baeder, [11] and[12], Sitaraman et al. [13], Zhan and Qian, [14] and[15]), which adopts the grid speed technique to simulate the velocity change of the flow field, has been successfully applied to calculating the gust response of the airfoil/wing (Harish and Alex [16]; Raveh; Raveh et al., [17] and [18], Yang et al., [19]). This method is shown to be suitable for computation of step change in airfoils. Moreover, the method of conventional field velocity is usually used to calculate the indicial response by incorporating unsteady flow

conditions via grid movement in CFD simulations (Parameswaran and Baeder, [20](Singh and Baeder, [21]). The main privilege of this method is the direct calculation of aerodynamic responses to step changes in flow conditions. An impulsive change in the angle-of-attack can be considered as an impulsive superposition of a uniform velocity field in the free stream. Besides, the magnitude of the indicial change for the angle of attack is used for the calculation of the magnitude of normal velocity. In this method, the necessity of uniform distribution of time step over the entire flow domain is guaranteed. In addition, the airfoil is not made to pitch. Hence, the influence of pure angle-of-attack and pitch rate are decoupled efficiently. A similar methodology for simulating responses of an airfoil to step changes in pitch rate and interaction with vertical gusts also exists. Moreover, the field velocity method is also applied for prediction of the effects of the trailed vortex wake from the other rotor blades in helicopters, compressors or other turbo machineries. A time dependence study illustrates that a smooth and accurate solution in time requires the consistent evaluation of time metrics in order to satisfy the geometric constitutive law (Sitaraman et al., [22]).

The objective of the present work is to investigate the unsteady transonic inviscid and viscous flow fields over a pitching or heaving NACA0012 airfoil at various angles of attack. A pressure based implicit procedure to solve the Euler and Navier-Stokes equations is developed in order to predict flows around the oscillation airfoil with a high resolution scheme. In this process, nonorthogonal and non moving mesh with collocated finite volume formulation are used. In order to simulate the pitching or heaving airfoil, oscillation of flow boundary condition is applied. The boundedness criteria for this procedure are determined from the Normalized Variable Diagram (NVD) scheme. The procedure incorporates the $k\text{-}\varepsilon$ eddy-viscosity turbulence model. The algorithm is then tested for inviscid and turbulent transonic aerodynamic flows around an oscillating airfoil. The results of the present study are compared with the other existing numerical solutions and with the experiment data. The comparisons show that the resolution quality of the developed algorithm is significant.

GOVERNING EQUATIONS AND DISCRETIZATION

The basic equations, which describe conservation of mass, momentum and scalar quantities, can be expressed in Cartesian tensor form as:

$$\frac{\partial}{\partial t}(\rho) + \frac{\partial}{\partial x_i}(\rho u_i) = 0 \tag{1}$$

$$\frac{\partial}{\partial t}(\rho u_i) + \frac{\partial}{\partial x_j}(\rho u_i u_j - T_{ij}) = S_i^u \qquad (2)$$

$$\frac{\partial}{\partial t}(\rho \phi) + \frac{\partial}{\partial x_i}(\rho u_i \phi - q_i) = S^\phi \qquad (3)$$

The stress tensor and scalar flux vector are usually represented in terms of basic dependent variable. The stress tensor for a Newtonian fluid is:

$$T_{ij} = -\left(P + \frac{2}{3}\mu\frac{\partial u_k}{\partial x_k}\right)\delta_{ij} + $$
$$\mu\left(\frac{\partial u_i}{\partial x_j} + \frac{\partial u_j}{\partial x_i}\right) \qquad (4)$$

The scalar flux vector usually given by the Fourier-type law is:

$$q_i = \Gamma_\phi\left(\frac{\partial \phi}{\partial x_i}\right) \qquad (5)$$

Turbulence is accounted for by adopting $k - \varepsilon$ turbulence model. The governing equations for these quantities are:

$$\frac{\partial}{\partial t}(\rho \kappa) + \frac{\partial}{\partial x_i}\left(\rho u_i k - \Gamma_k\frac{\partial k}{\partial x_i}\right)$$
$$= G - \rho \varepsilon + D_{comp} + \Theta_{diff} \qquad (6)$$

$$\frac{\partial}{\partial t}(\rho \varepsilon) + \frac{\partial}{\partial x_i}\left(\rho u_j \varepsilon - \Gamma_\varepsilon\frac{\partial \varepsilon}{\partial x_i}\right)$$
$$= +C_{1\varepsilon}\frac{\varepsilon}{\kappa}G - C_{2\varepsilon}\rho\frac{\varepsilon^2}{\kappa} \qquad (7)$$

The turbulent viscosity and diffusivity coefficients are defined by

$$\mu_t = C_\mu\rho\frac{k^2}{\varepsilon} \qquad (8)$$

$$\Gamma_\phi^t = \left(\frac{\mu_t}{\sigma_\phi^t}\right) \qquad (9)$$

and the generation term G in eqs. 0 and 0 is defined by

$$G = \mu_t\left(\begin{bmatrix}\frac{\partial U_i}{\partial x_j} + \frac{\partial U_j}{\partial x_i}\end{bmatrix}\frac{\partial U_i}{\partial x_j} - \frac{2}{3}\delta_{ij}\begin{bmatrix}\frac{\partial U_l}{\partial x_l} + \rho k\end{bmatrix}\frac{\partial U_l}{\partial x_l}\right) \qquad (10)$$

The term D_{comp} and Θ_{diff} are additional contributions to the standard $k - \varepsilon$ model often introduced to account for the effects of compressibility [23,24]. In this work, the models proposed by Yang et al., [23] are adopted, namely,

$$D_{comp} = -\frac{9}{55}\rho k\frac{\partial u_i}{\partial x_i} -$$
$$\frac{1}{\rho}\cdot\frac{\mu_t}{\rho}\cdot\frac{\partial \rho}{\partial x_i}\frac{\partial p}{\partial x_i} \qquad (11)$$

$$\Theta_{diff} = 0 \qquad (12)$$

The latter being appropriate for high Reynolds number flows, as it is the case here. The values of the turbulence model coefficients used in the present work are given in Table 1 (Yang et al., [23]).

Table 1. Values of emperical coefficients in the standard k-ε turbulence model

C_1	C_2	$C\mu$	σ_k	σ_ε
1.44	1.92	0.09	1.0	1.3

The discretization of the above differential equations is carried out using a finite-volume approach. First, the solution domain is divided into a finite number of discrete volumes or cells, where all variables are stored at their geometric centers (see e.g. Fig. 1). The equations are then integrated over all the control volumes by using the Gaussian theorem. The development of the discrete expressions to be presented is effected with reference to only one face of the control volume, namely, *e*, for the sake of brevity.
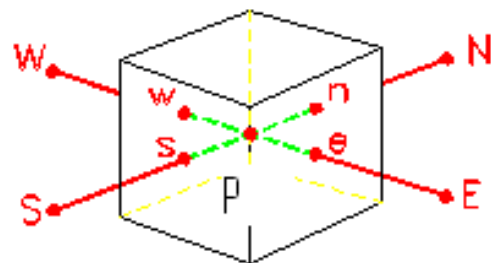

Figure 1. Finite volume and storage arrangement

For any variable ϕ (which may now also stand for the velocity components), the result of the integration yields

$$\frac{\delta \upsilon}{\delta t}[(\rho\phi)_p^{n+1} - (\rho\phi)_p^n] + I_e - I_w$$
$$+ I_n - I_s = S_\phi \delta\upsilon \qquad (13)$$

$$I_e^D = D_e(\phi_p - \phi_E) - S_e^\phi \qquad (14)$$

where $I_{(S)}$ is the combined cell-face convection I^C and diffusion I^D fluxes. The diffusion flux is approximated by central differences and can be written for cell-face *e* of the control volume in Fig.1, as an example, as:

where S_e^ϕ stands for the cross derivative arising from mesh nonorthogonality. The discretization of the convective flux, however, requires special attention and is the subject of the various schemes developed. A representation of the convective flux for cell-face e is:

$$I_e^c = (\rho.V.A)_e \phi_e = F_e \phi_e \qquad (15)$$

The value of the dependent variable ϕ_e is not known and should be estimated using an interpolation procedure, from the values at neighboring grid points. ϕ_e is determined by the SBIC scheme (Djavareshkian [25]), that it is based on the NVD technique, used for interpolation from the nodes E, P and W. So the expression can be written as:

$$\phi_e = \phi_W + (\phi_E - \phi_W).\widetilde{\phi}_e \qquad (16)$$

The functional relationship used in SBIC scheme for $\widetilde{\phi}_e$ is given by:

$$\widetilde{\phi}_e = \widetilde{\phi}_P \qquad \text{if} \quad \tilde{\varphi}_P \le 0 \text{ or } \tilde{\varphi}_P \ge 1$$

$$\tilde{\varphi}_e = -\frac{\tilde{x}_P - \tilde{x}_e}{K(\tilde{x}_P - 1)} \tilde{\varphi}_P^2$$

$$+ \left(1 + \frac{\tilde{x}_P - \tilde{x}_e}{K(\tilde{x}_P - 1)}\right) \tilde{\varphi}_P \qquad \text{if} \quad 0 < \widetilde{\phi}_P < K \qquad (17)$$

$$\widetilde{\phi}_e = \frac{\widetilde{x}_P - \widetilde{x}_e}{\widetilde{x}_P - 1} + \frac{\widetilde{x}_e - 1}{\widetilde{x}_P - 1} \widetilde{\phi}_P \qquad \text{if} \quad K \le \widetilde{\phi}_P < 1$$

$$0 < K \le 0.5$$

where

$$\tilde{\varphi}_P = \frac{\varphi_P - \varphi_W}{\varphi_E - \varphi_W} \quad \tilde{\varphi}_e = \frac{\varphi_e - \varphi_W}{\varphi_E - \varphi_W}$$

$$\tilde{x}_e = \frac{x_e - x_W}{x_E - x_W} \quad \tilde{x}_P = \frac{x_P - x_W}{x_E - x_W} \qquad (18)$$

The limits on the selection of each value of K can be determined in the following way. Obviously the lower limit is to keep $K = 0$, which would represent switching between upwind and central differencing. This should not be favored because; it is essential to avoid the abrupt switching between the schemes in order to achieve the converged solution. The upper limit of K is 0.5, since it represents the constant gradient and there is no need to use anything other than central differencing in that case. The value of K should be kept as low as possible in order to achieve the maximum resolution of the scheme. According to Eq. (17), if $\widetilde{\phi}_P$ (or $\widetilde{\phi}_C$ normalized variable at the central node) does not belong to [0,1], the space discretization is first order, otherwise the SBIC scheme

has second order accuracy from the point of view of space discretization. The details of how the interpolation is made are dealt with([25]); it would suffice here to say that the discretized equations resulting from each of the approximations take this form:

$$A_P.\phi_P = \sum_{m=E,W,N,S} A_m.\phi_m + S'_\phi \qquad (19)$$

where $A_{(s)}$ are the convection-diffusion coefficients. The term S'_ϕ in Eq.· contains quantities arising from non-orthogonality, numerical dissipation terms, external sources, deferred correction terms, and $(\rho \delta \upsilon / \delta t)\phi_P$ of the old time-step/iteration level. For the momentum equations, it is easy to separate out the pressure-gradient source from the convected momentum fluxes.

SOLUTION ALGORITHM

The set of Eq. (19) is solved for the primitive variable (velocity components and energy) together with continuity utilizing pressure-based implicit sequential solution methods. The technique used is the PISO scheme presented herein (Issa, [26]). In this technique, the methodology has to be adapted to handle the way in which the fluxes are computed in Eqs. (15-18). The adapted PISO scheme consists of a predictor and two corrector sequence of steps at every iteration. The predictor step solves the implicit momentum equation using the old pressure field. Thus, for example, for the u component, the momentum predictor stage can be written as

$$u^* = H(u^*) - D\nabla p^o + S'_u \qquad (20)$$

where H contains all terms relating to the surrounding nodes and superscripts; while, * and o denote intermediate and previous iteration values, respectively. Note that the pressure-gradient term now written out explicitly, is extruded from the total momentum flux by simple subtraction and addition. The corrector-step equation can be written as:

$$u^{**} = H(u^*) - D\nabla p^* + S'_u \qquad (21)$$

Hence, from Eqs. (20) and (21)

$$u^{**} - u^* = -D\nabla(p^{**} - p^*) \quad or \quad \delta u = -D\nabla \delta p \qquad (22)$$

Now the continuity equation demands that

$$\frac{\delta \rho}{\delta t} + \nabla(\rho^* u^{**}) = 0 \qquad (23)$$

For compressible flows it is essential to account for the effect of change of density on the

mass flux as the pressure changes. This is accounted for by linearizing the mass fluxes as flows

$$\rho^* u^{**} \approx \rho^o u^* + \rho^o \delta u + u^* \delta \rho$$

or (24)

$$\rho^* u^{**} \approx \rho^o u^* - \rho^o D \nabla \delta p + u^* (\frac{d\rho}{dp}) \delta p$$

where Eq. (22) is invoked to eliminate δu, and $\delta \rho$ is related to δp by the appropriate equation of state. Substitution of Eq. (24) into Eq. (23) yields a pressure-correction equation of the form

$$\mathbf{A_P}.\delta \mathbf{p_P^*} = \mathbf{A_E}.\delta \mathbf{p_E^*} + \mathbf{A_W}.\delta \mathbf{p_W^*} + \mathbf{A_N}.\delta \mathbf{p_N^*} + \mathbf{A_S}.\delta \mathbf{p_S^*} + \mathbf{S_P} \quad (25)$$

where S_P is the finite difference analog of $\nabla(\rho^o u^*)$, which vanishes when the solution is converged. The A coefficients in Eq. (25) take the form of (the expression for A_E is given as an example):

$$A_E = (\rho^o \tilde{a} D)_e - \lambda_e (\tilde{a} u^*)_e.(\frac{d\rho}{dp})_e \quad (26)$$

where λ is a factor the significance of which is to be explained subsequently. The mass flux at a cell face is computed from nodal values of density and velocity, but the cell-face values of ρ_e^o and u_e^* in Eq. (26) are not readily available. To compute those values, assumptions concerning the variations of ρ need to be made. In upwinding $\lambda = 1$ when u is positive; otherwise it would be zero. Alternatively, in central difference formula $\lambda = 1/2$.

Such assumptions have no influence whatsoever on the final solution because they affect only the pressure-correction coefficients, and as δp approaches zero at convergence, the solution is, therefore, independent of how those coefficients are formulated; however, they do influence the convergence behavior.

The structure of the coefficients in Eq. (25) simulates the hyperbolic nature of the equation system. Indeed, a closer inspection of expression (26) would reveal an upstream bias of the coefficients (A decreases as u increases), and this bias is proportional to the square of the Mach number. Also, note that the coefficients reduce identically to their incompressible form in the limit of zero Mach number.

In the present work, Crank-Nicolson scheme [26] is applied for discretization of time derivative with second order accuracy. This option seems to be the most obvious as it requires the minimum amount of memory storage of the velocity fields (Barton, 1998). It should be noted that the system of equation is solved using biconjugation method.

BOUNDARY CONDITIONS

At the inlet of the domain, only three of the four variables need to be prescribed: the total temperature, the angle of attack, and the total pressure. The pressure is obtained by zeroth order extrapolation from interior points. At the outlet, pressure is fixed. Slip boundary conditions are used on the lower and upper walls. In the case of viscous flow, the non-slip condition is applied to the airfoil surfaces. To account for the steep variations in turbulent boundary layers near solid walls, wall functions, which define the velocity profile in the vicinity of no-slip boundaries, are employed. The far-field boundary is set at 30c from the airfoil to minimize its undesired effects on the flow surrounding and to be in accordance with slip boundary conditions.

RESULTS AND DISCUSSION

PITCHING PART

In this section, the results of the inviscid and viscous flows over a pitching NACA0012 airfoil along its quarter chord axis are presented. The simulations are performed at a higher Reynolds number. In particular, we aim to validate the simulation with the help of the existing experiment results of a pitching airfoil, and also study the lift and drag characteristics of this airfoil. The steady state solutions are used as initial conditions for time-marching calculations. Fig. 2 provides an illustration of pure-pitch motion for an airfoil with a mean angle of attack of α_m. The parameters of motion and flow field are also described in Table 2. The airfoil is forced into an oscillation around an axis located at the quarter-chord. The angle of attack is specified as:

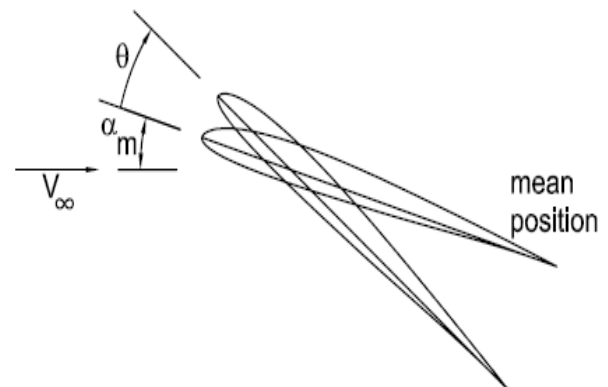$$\alpha(t) = \alpha_m + \alpha_p \sin(\omega_\alpha t) \quad (27)$$

Figure 2. Pure pitch definition

Table 2. Pure pitch motion parameters

κ	M_∞	α_m (deg.)	α_p (deg.)	c
0.0814	0.755	0.016	2.51	1.0

The free stream velocities for unsteady computations are set at $u_{inlet}=u_\infty\cos(\alpha(t))$ and $v_{inlet}=u_\infty\sin(\alpha(t))$. An H-type mesh is generated to model the airfoil and the surrounding flow. The schematic of this grid which is used in the present simulation is shown in Fig. 4. The grid dependence test for Navier-Stokes Equation on the NACA0012 airfoil at $M_\infty= 0.755$, $\alpha= -1.8°$ is indicated in Fig.5. Three different mesh sizes are considered: 27680, 57950 and 115960 cells and each simulation emerges from its fully converged solution. Thus the mesh of 57980 cells is selected as a baseline mesh for further analyses. Figes. 6 (a)-(c) compare the computed viscous case surface pressure distribution with the experimental data [27] on NACA0012 with $M_\infty=0.755$, $\alpha_m=0.016°$, $\alpha_p=2.51°$, $k=0.0814$ for two angles of attacks. As it can be realized from these results, there is quite a good agreement between the present method and the measurement of Landon [27]. These comparisons show that the solutions using oscillating boundary condition method enjoy an acceptable prediction.
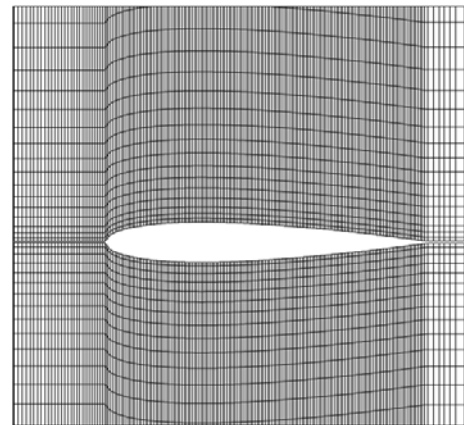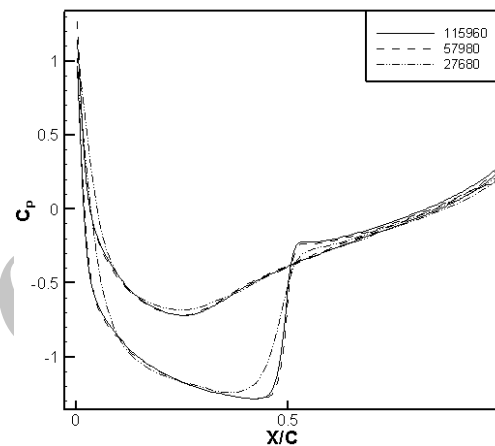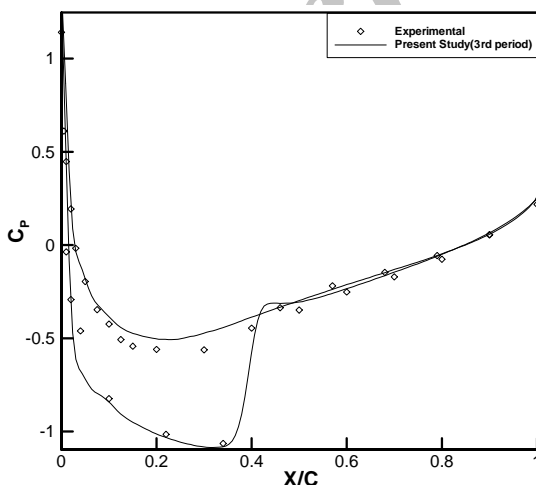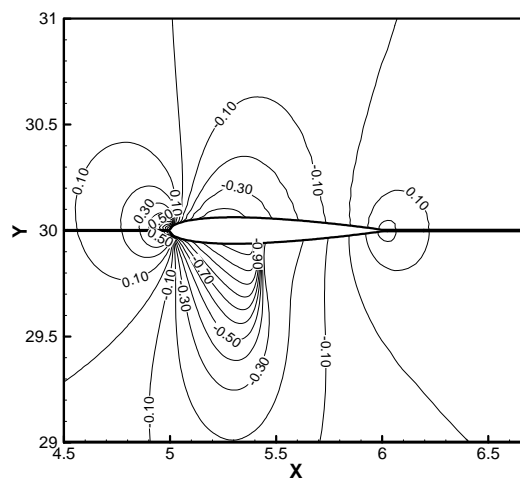

Figure 4. Part of the H grid

Figure 5. Grid dependency results for NACA0012, $M_\infty=$ 0.755, $\alpha= -1.8°$

a) $\alpha(t)=-0.54°$

b) Pressure coefficient distribution $\alpha(t)=)=-0.54°$

c) α(t)=2.34˚
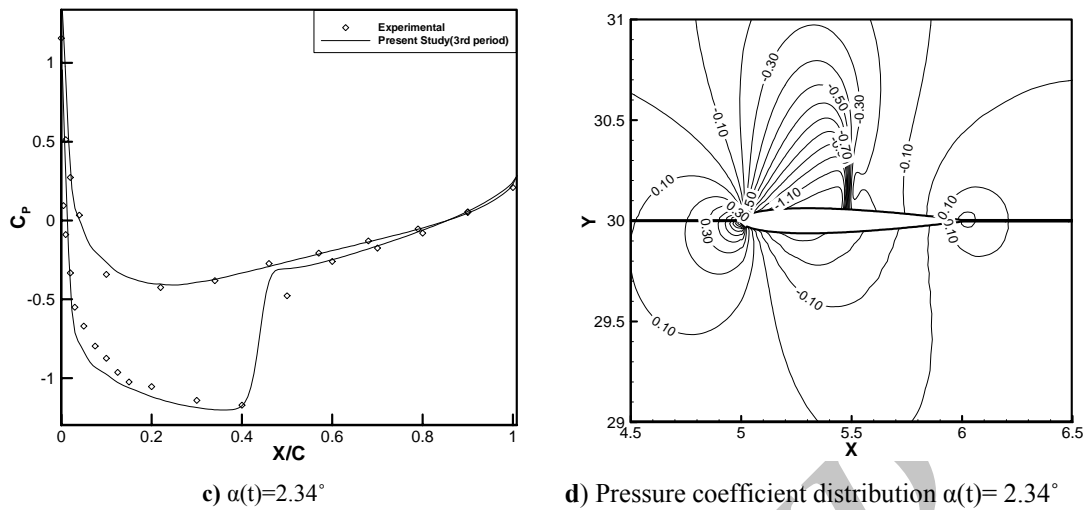

d) Pressure coefficient distribution α(t)= 2.34˚

Figure 6. Pressure distribution on NACA0012, M_∞=0.755, α_m=0.016˚, α_p=2.51˚, k=0.0814

The computed variation of the lift coefficient versus angle of attack for inviscid and viscous flows during the third cycle is compared with that of Uzun [28] and Landon [27] in Fig. 7 (a) and (b). The existence of this variation loop is the result of induced velocities, which result in different lift coefficients between the up and downstrokes. For the presented viscous case, the turbulence quantities were specified at inlet to correspond to 0.008 turbulence intensity and a dissipation length scale of 10% of the airfoil chord. The value of K in SBIC scheme for this case is 0.3. Fig. 7(a) shows the computed variation of lift coefficient versus the angle of attack for viscous case which is in close agreement with experimental data. Difference between the

experimental data and numerical simulation results of this research can be caused by several factors a) solution algorithm, in pressure based algorithm , the segregated method is used to solve discretized equations and the internal and external loop number can affect the results, b) Eddy viscosity models can affect unsteady airload hysteresis loops c) Experimental data can be the same as combined error, and d) In the present work, non moving mesh is employed and in order to simulate a pitching or heaving airfoil, oscillation of flow boundary condition is applied; but in the experimental test, the airfoil is oscillating. Fig. 7 (b) shows the C_l versus α for inviscid case.
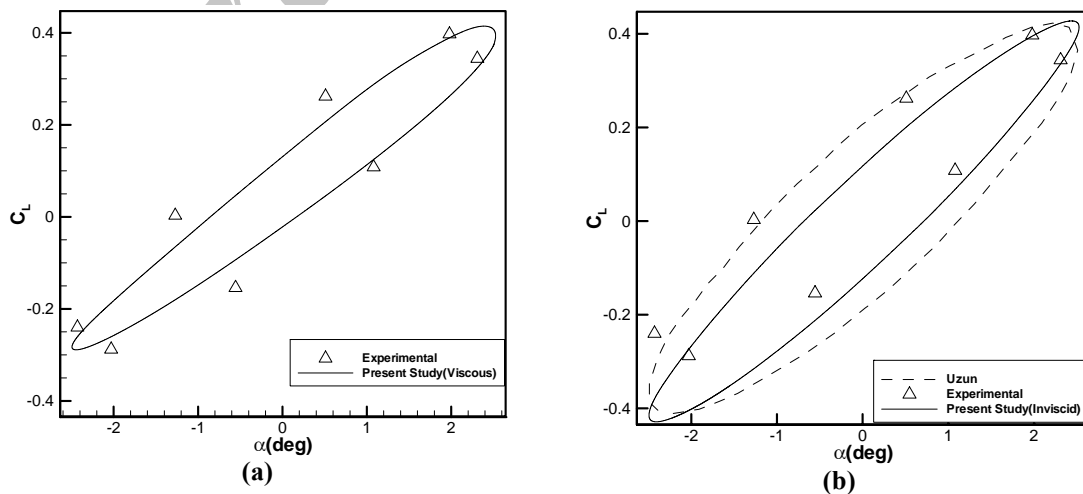

(a)

(b)

Figure 7. Lift coefficient versus angle of attack for M_∞=**0.755**, α_m=**0.016**˚, α_p=**2.51**˚, k=0.0814 a) viscous case b)

invicid case

Uzun [28] used a parallel algorithm for the solution of unsteady Euler equation on unstructured reformatting grids while in this study the non moving mesh with oscillation of flow boundary condition is applied. It can be seen that neither of these methods are in good agreement with the experimental data, particularly at the lowest angle of attack. The reason for this difference is caused by the lack of consideration of viscosity. In other words, the viscosity can impact the separated vortex from the airfoil and aerodynamic coefficients in an unsteady flow.

The predicted drag coefficients versus the angle of attack are illustrated in Fig.8. The upstroke C_d and C_{dmin} are higher than the downstroke one. This is explained by the aerodynamic phase lag, i.e. the strong influence of the shed vortices in the wake on the bound-airfoil circulation. Details of these unsteady (circulatory) effects are described by Leishman [29] and Cebeci– et al. [30] in the context of attached aerodynamics.In this work, the effect of the airfoil amplitude of oscillation on the simulated lift coefficients is assessed. The instantaneous C_L versus τ where K=0.0184, M=0.755 on NACA0012 is depicted in Fig. 9. As illustrated, the maximum lift coefficients increase at higher amplitudes of oscillation. Besides, the calculated lift coefficients are periodic and resemble harmonic-like patterns. Furthermore, increasing the amplitude endues significant lead in the C_L results that $C_{L\max}$ is obtained at a lower τ. This can be attributed to the stronger effects of the shed wake and the vertical structures on the surrounding fluid in the higher amplitudes.
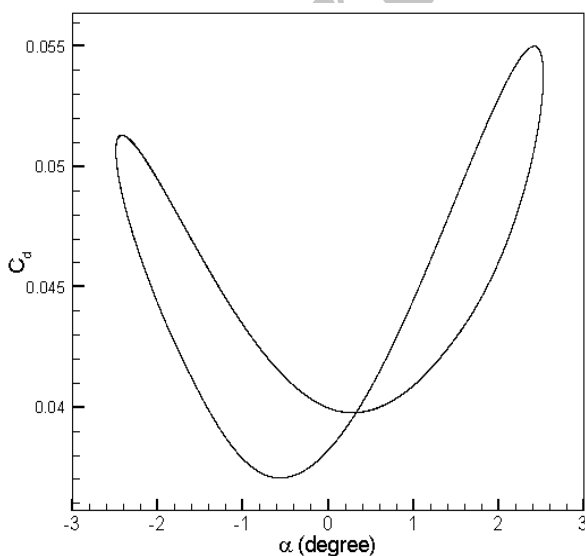

Figure 8. Drag coefficient versus angle of attack for viscous case at M_∞=0.755, α_m=0.016˚, α_p=2.51˚, k=0.0814
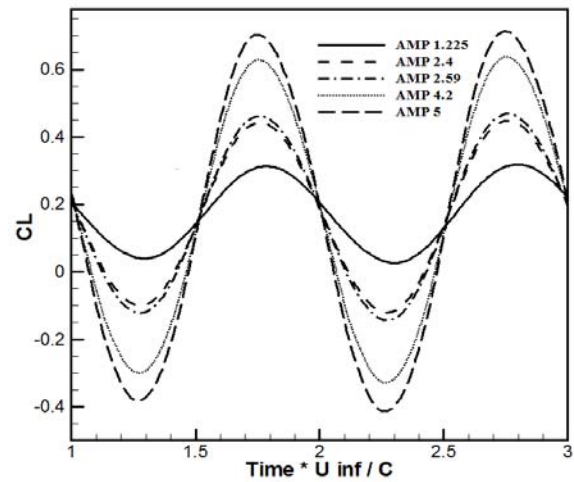

Figure 9. Instantaneous Lift coefficient versus non-dimensional time M_∞=0.755, k=0.0814

HEAVING PART

In this section, the results of the viscous flows over a Heaving NACA0012 airfoil are indicated. The simulations are performed at a higher Reynolds number. In particular, we aim to validate the simulation with the existing numerical results of a heaving airfoil, and study its lift characteristics. The steady state solutions at 1° angle of attack are used as initial conditions for the time-marching calculations. The non-slip boundary condition is applied along the airfoil surface. The far-field boundary is also set at 30c from the airfoil to minimize its undesired effects on the flow surrounding and is accordance with the slip boundary conditions. Fig. 10 provides an illustration of a pure-heaving motion. The parameters of motion and flow field are described in Table 3. The heaving velocity of the sinusoidal motion is given as:

$$v_o(t) = -M_\infty . \sin\left(\frac{\pi}{180}\right). \sin\left(\omega(t - \Delta t)\right) \qquad (28)$$

$$v_o(t) = \frac{\dot{h}(t)}{a_\infty} \qquad (29)$$
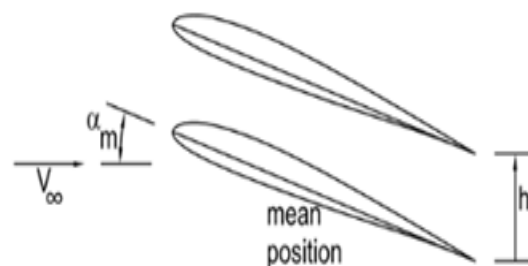
$$\Delta t = \frac{L}{U\infty} \qquad (30)$$

Figure 10. Pure plunge motion definition, α_m=1°

Table 3. Pure heaving motion parameters

κ	M_∞	c
0.2	0.8	1.0

The significant point in the simulation of heaving airfoil with oscillation boundary condition is to consider a lag phase (Δt). Eq. 28 has been non-dimensionalized by the free stream speed of sound a_∞. The free stream velocities for unsteady computations are set at $u_{inlet}=U_\infty$ and $v_{inlet}=U_\infty \sin(\alpha(t))$. An H-type mesh is generated to model the airfoil and the surrounding flow. The schematic of the grid which is used in the present simulation is shown in Fig. 4. The computed variation of the lift coefficient versus the angle of attack for viscous flows during the third cycle is compared with that of Uzun [28] and Lin [27] in Fig. 11. For the presented viscous case, the turbulence quantities are specified at inlet to correspond to 0.008 turbulence intensity and a dissipation length scale of 10% of the airfoil chord. The value of K in SBIC scheme for the case of validation is 0.05. This figure shows the computed variation of lift coefficient versus the angle of attack for viscous case, which is in a close agreement with the published results. Uzun [27] used dynamic mesh with a parallel algorithm for the solution of unsteady Euler equation on unstructured reformatting grids while in this study a nonmoving mesh with oscillation of flow boundary condition is applied. Moreover, Lin used multi reference frame for the simulation of heaving motions. This comparison shows the resolution of these methods is considerable. Although the present method is simple and has low cost for calculation, the dynamic mesh and the multi references of frame method are both time consuming and very complicated to develop. Fig. 12 demonstrates the effect of SBIC parameter (k) on the lift coefficient at α=1°, M=0.8, and κ=0.2 for NACA0012. As it can be seen, the value of the different k coefficients does not have so much effect on the resolution of the solution.
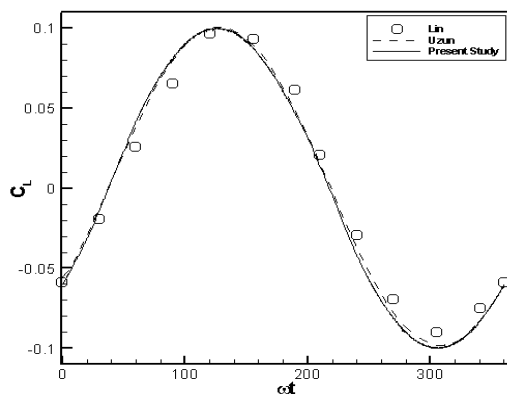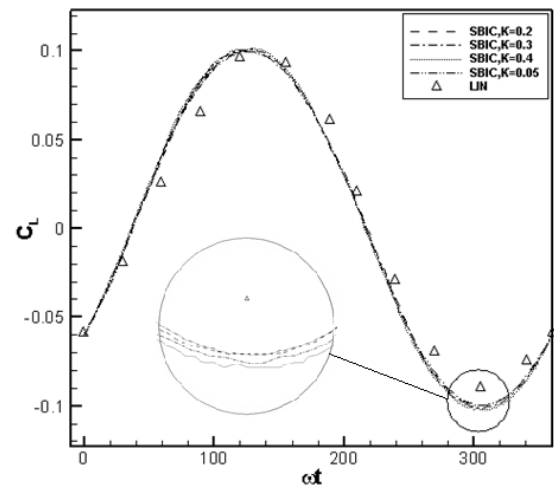

Figure 11. Lift coefficient distribution for Pure Heaving Motion, M=0.8, κ=0.2, NACA0012

Figure 12. Effect of SBIC parameter (k) on Lift coefficient, α=1°, M=0.8, κ=0.2, :NACA0012

Fig.13 shows different flowcharts for Time advancement and Table 4 indicates CPU Time comparison for different internal and external loop iterations. The numbers of iteration to satisfy the convergence criteria for the external loops of algorithms (a), (b) and (c) are approximately1000, 0 and 1-2, respectively and these numbers for the internal loops of these algorithms are about 0, 20-30 and 2-3 respectively. As a result, the two algorithms (a) and (b) are time consuming, but CPU time for (c) method is considerably decreased.

Table 4. CPU Time comparison for different algorithms

	Iterative Algorithm	Non-Iterative Algorithm	presented Algorithm
Internal Loop No.	-	20-30	3-5
External Loop No.	500	-	2-3
CPU Time (min)	5000	2000	180

CONCLUSIONS

A pressure based implicit procedure to solve the Euler and Navier-Stokes equations is developed to predict transonic viscous and inviscid flows around the pitching and heaving airfoil with a high resolution scheme. In order to simulate a moving airfoil, oscillation of flow boundary condition is applied. The boundedness criteria for this procedure are determined from Normalized Variable Diagram (NVD) scheme. The main findings can be summarized as follows: (1)- The moving airfoil simulation with the oscillation of flow boundary condition with fix grid is very simple and has low cost. (2)- The grid dependence test with high resolution scheme indicates that an acceptable solution can be obtained even on a fairly coarse 3-the agreement

between numerical and experimental data is considerable, and (4)- The CPU time for the presented method is considerably reduced.
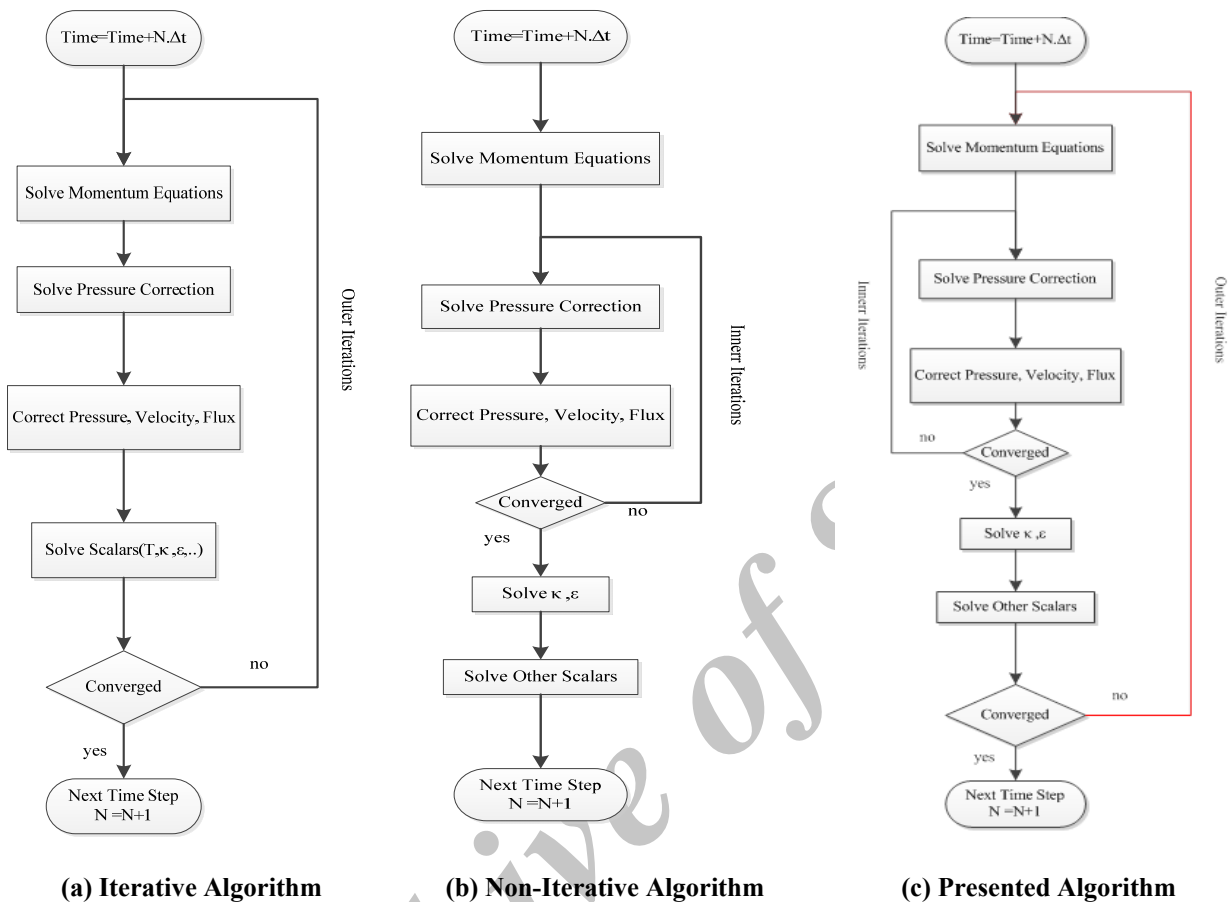

(a) Iterative Algorithm   **(b) Non-Iterative Algorithm**   **(c) Presented Algorithm**

Figure 13. Different Flowcharts for Time advancement

REFERENCES

1. Shankar, V., Ide, H., 1988, Aeroelastic computations of flexible configurations, Computers & amp; Structures 30, pp.15-28.

2. Goswami, A., Parpia, I.H., 1991, Grid Restructuring for Moving Boundaries, AIAA-91-1589-CP.

3. Batina, J.T., 1990. Unsteady Euler airfoil solutions using unstructured dynamic meshes. AIAA Journal 28, pp. 1381-1388.

4. Zheng, Y., Lewis, R.W., Gethin, D.T., 1996, Three-dimensional unstructured mesh generation: Part 1, Fundamental aspects of triangulation and point creation, Computer Methods in Applied Mechanics and Engineering 134, pp. 249-268.

5. Nakahashi, K., Deiwert, G.S., 1987, Self-adaptive-grid method with application to airfoil flow. AIAA Journal 25, pp. 513-520.

6. Levine, M., Williams, M., Whitlow, W., 1988. Body Conforming Grids for General Unsteady Airfoil Motion, Structures, Structural Dynamics and Materials Conference; 29th, Williamsburg, VA; United States pp. 530-540.

7. Guruswamy, G.P., 1990, Unsteady aerodynamic and aeroelastic calculations for wings using Euler equations. AIAA Journal 28, pp. 461-469.

8. Lohner, R., 1988, An adaptive finite element solver for transient problems with moving bodies, Computers & amp; Structures 30, pp. 303-317.

9. Farhat, C., Lin, T.Y., 1990, Transient Aeroelastic Computations Using Multiple Moving Frames of Reference. AIAA Journal, pp. 953-965.

10. Parameswaran, V., Baeder, J.D., 1997, Indicial aerodynamics in compressible flow-direct computational fluid dynamic calculations. American Institute of Aeronautics and Astronautics, Reston, VA, ETATS-UNIS.

11. Singh, R. and Baeder, J., 1963, Transonic effects on acoustics of blade-vortex interaction, Archive Set 748, American Institute of Aeronautics and Astronautics.

12. Singh, R., Baeder, J.D., 1997, Direct calculation of three-dimensional indicial lift response using computational fluid dynamics, American Institute of Aeronautics and Astronautics, Reston, VA, ETATS-UNIS.

13. Sitaraman, J., Baeder, J. and Iyengar, V., 2003, On the Field Velocity Approach and Geometric Conservation Law for Unsteady Flow Simulations, 16th AIAA Computational Fluid Dynamics Conference, American Institute of Aeronautics and Astronautics.

14. Zhan, H., Qian, W.-q., 2007, Numerical simulation of gust response for airfoil and wing, Acta, Aerodynamic, Sinica 25, pp. 531-536.

15. Zhan, H., Qian, W.-q., 2009, Numerical simulation on gust response of elastic wing, Chinese Journal of Computational Mechanics 26, pp. 270-275.

16. Harish, G., Alex, P., 2008, A Numerical Study of Gust Suppression by Flapping Airfoils, 26th AIAA Applied Aerodynamics Conference.

17. Raveh, D.E., 2011, Gust-Response Analysis of Free Elastic Aircraft in the Transonic Flight Regime. Journal of Aircraft Vol. 48, No. 4, pp. 1204-1211.

18. Raveh, D.E., Liu, D.D., Strganac, T.W., Dowell, E.H., Silva, W.A., Beran, P.S., 2007, CFD-Based Models of Aerodynamic Gust Response. Journal of Aircraft 44, pp. 888-897.

19. Yang, G., Obayashi, S., Guruswamy, G.P., 2004, Numerical Analyses of Discrete Gust Response for an Aircraft. Journal of Aircraft 41, pp. 1353-1359.

20. Parameswaran, V., Baeder, J.D., 1997, Indicial aerodynamics in compressible flow-direct computational fluid dynamic calculations. American Institute of Aeronautics and Astronautics, Reston, VA, ETATS-UNIS.

21. Singh, R., Baeder, J.D., 1997, Direct calculation of three-dimensional indicial lift response using computational fluid dynamics. American Institute of Aeronautics and Astronautics, Reston, VA, ETATS-UNIS.

22. Sitaraman, J., Baeder, J., Iyengar, V., 2003, On the Field Velocity Approach and Geometric Conservation Law for Unsteady Flow Simulations, 16th AIAA Computational Fluid Dynamics Conference. American Institute of Aeronautics and Astronautics.

23. Yang, Z.Y., Chin, S.B., Swithenbank, J., 1991, On the Modeling of the k-equation for Compressible flow, 7th International Symposium on numerical methods in laminar and turbulent flow, Stanford, CA.

24. Narayam, J.R, and Sekar, B., 1991, Computational of Turbulent High Speed Mixing Layers Using a Two-equation Turbulence Model, CFD symposium on aeropropulsion, NASA CP-3078, Jan.

25. Djavareshkian, M.H., 2004 Pressure-based compressible calculation method utilizing normalized variable diagram scheme, Iranian Journal of Science and Technology, Volume 28, Number B4, pp. 495-500

26. Issa, R.I., 1986, Solution of the implicitly discretised fluid flow equations by operator-splitting, Journal of Computational Physics 62, pp.40-65.

27. Landon, R.H., 1982, NACA 0012 Oscillating and Transient Pitching, in AGARD Report.

28. Uzun, A. 1999, Parallel Computations Of Unsteady Euler Equations On Dynamically Deforming Unstructured Grid. Msc Thesis, Purdue University

29. Leishman, J. G., Principles of Helicopter Aerodynamics, 2nd ed., Cambridge Univ. Press, New York, 2006.

30. Cebeci, T., Platzer, M., Chen, H., Chang, K., and Shao, J. P., Analysis of Low-Speed Unsteady Airfoil Flows, Springer, Heidelberg, Germany, 2005.